RSC Advances

PAPER

View Article Online
View Journal | View Issue

Cite this: *RSC Adv.*, 2026, **16**, 12816

Eco-friendly AuNPs@rGO nanocomposite as a peroxidase-mimic for cholesterol detection

Wafa Al-Gethami,[a] Mohammad Shariq, *[b] Vijay Kumar,[c] Eman Alzahrani,[a] Ohoud F. Al Sharif,[a] Mona Mohammad AlAmri,[d] Mukul Sharma,[e] Raha Osailan,[f] Dalin A. Hassan[g] and A. Khatab[hi]

This study presents the development of an artificial enzyme based on a nanocomposite composed of green-synthesized gold nanoparticles (AuNPs) and reduced graphene oxide (rGO), (AuNPs@rGO), for the selective and sensitive colorimetric detection of cholesterol (ChO). The nanocomposite exhibits peroxidase-like activity, catalyzing the oxidation of tetramethylbenzidine (TMB) into a blue-colored oxidized product (oxTMB) *via* hydroxyl radical (•OH) generation. Cholesterol Oxidase (ChOx) enzymatically oxidizes cholesterol to produce hydrogen peroxide (H_2O_2) and cholest-4-en-3-one, and the resulting H_2O_2 is subsequently utilized by AuNPs@rGO to oxidize TMB. The nanocomposite was synthesized by integrating green-synthesized AuNPs with rGO prepared through a modified Hummers' method. Characterization using TEM, FTIR, and XRD confirmed the successful fabrication and structural features of AuNPs@rGO. The system demonstrated a linear response for cholesterol concentrations ranging from 0.2 to 1.2 mM, with a high correlation coefficient (R^2 = 0.996) and a low limit of detection (LOD = 0.062 mM). These findings underscore the potential of AuNPs@rGO as a robust, efficient, and cost-effective platform for cholesterol sensing, offering a promising approach for diagnostic and biomedical applications.

Received 4th October 2025
Accepted 18th February 2026

DOI: 10.1039/d5ra07564e

rsc.li/rsc-advances

1. Introduction

In recent years, the development of artificial enzymes, also known as mimetic nanoscale materials, has emerged as a groundbreaking approach for colorimetric detection. This innovation has garnered significant attention from researchers in biomaterials and biosensing.[1,2] Artificial enzymes offer numerous advantages over their natural counterparts, including superior stability across a wide range of pH and temperature conditions and heightened sensitivity.[3] Additionally, these enzymes are cost-effective and exhibit customizable catalytic activity, further solidifying their potential as a robust tool for colorimetric detection. Building on the pioneering report on artificial enzyme synthesis,[4] researchers have successfully engineered a diverse array of nanoscale materials with enzyme-like functionality, expanding the frontiers of biomimetic catalysis.[5] These include Co_3O_4,[6] CeO_2,[7] V_2O_5,[8] PdNPs,[9] PtNPs, AuNPs,[10–12] CNTs,[12] GO,[13] and CQDs.[14] Among these nanomaterials, AuNPs have garnered significant attention due to their remarkable biocompatibility, easy preparation, and impressive catalytic, optical, and electronic properties at the nanoscale.[15,16] However, the high cost of AuNPs and their tendency to aggregate at lower pH significantly limit their catalytic efficiency. Therefore, to reduce the cost of AuNP-based catalysis while improving dispersion and stability, it is crucial to immobilize green synthesized AuNPs on a suitable support material. Leaf extract-synthesized AuNPs offer notable advantages, such as enhanced stability, superior biocompatibility, cost-effective synthesis, and exceptional catalytic activity.

Graphene nanocomposites have garnered significant attention as SI due to their exceptional properties, including low cost, large surface area, excellent electrical and thermal conductivity, and remarkable reliability.[17–19] Previous studies have successfully demonstrated the dispersion of AuNPs over graphene sheets.[20,21] However, to our knowledge, only a few researchers have explored the AuNPs@rGO nanocomposite as an "artificial enzyme".[22,23]

[a]*Department of Chemistry, College of Science, Taif University, P.O. Box 11099, Taif, 21944, Saudi Arabia*

[b]*Department of Physics, Faculty of Science, Integral University, Lucknow 226026, India. E-mail: lucknow84iit@gmail.com; aligshariq@gmail.com*

[c]*Department of Environmental Science, Satyawati College, University of Delhi, Delhi-110052, India*

[d]*Department of Chemistry, College of Science, University of Bisha, Bisha 61922, Saudi Arabia*

[e]*Environment and Nature Research Centre, Jazan University, P.O. Box 114, Jazan, 45142, Saudi Arabia*

[f]*Department of Biology, College of Science, Taibah University, Yanbu, Saudi Arabia*

[g]*Department of Pharmacology and Toxicology, College of Pharmacy, Jazan University, Jazan 45142, Saudi Arabia*

[h]*Department of Physics, College of Science in Yanbu, Taibah University, Yanbu Governorate, Saudi Arabia*

[i]*Department of Laser Sciences and Interactions, National Institute of Laser Enhanced Sciences, Cairo University, Egypt*

Furthermore, there are currently no reports on using negatively charged AuNPs, synthesized *via* leaf extracts, as artificial enzymes.

The synergistic integration of graphene's large surface area with the unique properties of AuNPs synthesized from leaf extracts inspired us to develop the AuNPs@rGO nanocomposite and explore its artificial enzyme-like activity. Cholesterol, a vital steroid molecule, plays a fundamental role in cellular function.[24] It is essential for maintaining membrane fluidity and structural integrity across a range of physiological temperatures.[25] Beyond being the primary structural component of plasma membranes, cholesterol is also indispensable for the biosynthesis of vitamin D, steroid hormones, and bile acids.[26] Cells synthesize cholesterol from simple precursor molecules to fulfill essential biological needs. In humans, serum cholesterol levels typically range between 1.0 and 2.2 mM.[27] While cholesterol is crucial for maintaining physiological functions, its excessive production can lead to severe health complications, including arteriosclerosis, hypertension, malabsorption disorders, brain thrombosis, and myocardial infarction.[28] Consequently, the accurate quantification of cholesterol is critically important for applications such as clinical diagnosis, food safety, and environmental monitoring.[24] This underscores the necessity of developing advanced analytical techniques for rapidly and precisely detecting cholesterol. Various techniques have been developed to quantify cholesterol levels in human blood serum, including fluorescence-based assays,[29] liquid chromatography,[30] molecular imprinting polymer (MIP) technology,[31] electrochemical methods,[32] colorimetric enzymatic assays,[33] and gas chromatography.[34] While these methods offer high sensitivity and low detection limits, their widespread applicability is hindered by the need for specialized technical expertise, expensive instrumentation, and labor-intensive sample preparation procedures.[35] For example, chromatography (*e.g.*, GC/HPLC) offers high accuracy but suffers from poor portability, long analysis time, and high cost. Electrochemical methods provide miniaturization/portability advantages but often require complex electrode modification and may lack the visual simplicity of colorimetric detection. Therefore, there is an urgent need for the development of cost-effective, user-friendly sensors capable of rapidly and accurately detecting cholesterol.

Therefore, the current study was designed to develop an artificial enzyme based on AuNPs and reduced graphene oxide (AuNPs@rGO) nanocomposite for the selective and sensitive colorimetric detection of cholesterol. The nanocomposite was synthesized by integrating green-synthesized AuNPs with rGO. The AuNPs@rGO nanocomposite successfully demonstrated a linear response for cholesterol concentrations ranging from 0.2 to 1.2 mM, with a high correlation coefficient ($R^2 = 0.996$) and a low limit of detection (LOD = 0.062 mM). The results show that AuNPs@rGO can be a great platform for cholesterol sensing because it is strong, efficient, and inexpensive. This could be a great way to go for diagnostics and other biological uses.

2. Materials and methods

2.1 Chemicals and reagents

Loba chemicals supplied the precursor for the AuNPs, chloroauric acid ($AuCl_4 \cdot xH_2O$). Chemicals such as, cholesterol oxidase (Chox), hydrogen peroxide (H_2O_2), and tetramethylbenzidine (TMB) were purchased from Merck in India. Fresh *Croton bonpandianum* (*C. bonplandianum*) leaves were gathered from the Indian Institute of Technology (BHU) campus in Varanasi, India.

2.2 Green synthesis of NC-AuNPs

NC-AuNPs were synthesized using a similar route adopted to synthesize AuNPs.[21] In short, 2 mL of 0.8 mM $HAuCl_4 \cdot xH_2O$ was mixed with 2% (v/v) of aqueous extract of *C. bonplandianum* (AEC) dose for synthesis, and the mixture was then exposed to sunlight. The biosynthetic processes of AuNPs were conducted in both ambient sunlight and in dark condition to access the efficiency of sunlight's photo-catalytic action. While synthesizing NC-AuNPs, the incident solar radiation intensity was 66 300 lux and the ambient temperature was 39 °C when the sun was directly above. In the dark, the temperature was 34 °C and the light intensity was zero lumens. Until account for potential temperature and solar radiation fluctuations, the trials ran from noon until 2 pm. In only 16 minutes, the reaction mixtures left in the sun became a deep purple and formed a sharp peak. Even after 10 hours, the reaction mixes that were kept in the dark failed to produce the same degree of colour change. Therefore, in order to optimise the remaining process parameters, trials of AuNPs synthesis were conducted under circumstances of direct sunlight using a one constant at a time method. Optimal conditions were determined for parameters including sunlight exposure time, AEC inoculum dosages, and $HAuCl_4 \cdot xH_2O$ concentration. The produced NC-AuNPs were then re-dispersed in deionised water after being centrifuged for 15 minutes at 15 000 rpm to remove water-soluble compounds and other secondary metabolites. Vacuum drying was used to achieve the final mass of NC-AuNPs after four cycles of this method.

2.3 Preparation of reduced graphene oxide and graphene oxide

The GO was prepared for this study according to published studies.[36,37] In brief, the reaction was performed by adding 3 g of graphite powder to the 360 : 40 mL concentrated H_2SO_4/H_3PO_4 mixture. Subsequently, 15 g of $KMnO_4$ was added to the above reaction mixture. The final reaction mixture was then constantly agitated for 12 hours at 50 °C and cooled at room temperature. Further, the reaction mixture was transferred into 1 litre of distilled water (DW) in the ice bath. Subsequently, 3 mL H_2O_2 of 30% was mixed while continuously stirring for two hours. The last step was a 15 minute centrifugation run at 10 000 rpm on the finished product. The final product was collected and washed with 5% HCl many times. Finally, it was washed repeatedly using DW. The final washed solid substance to be cleaned, GO, was then put in a vacuum oven at 70 °C for a full day. After the synthesis of GO, rGO was prepared by suspending the resulting GO in DW (1 mg mL^{-1}) and thoroughly mixed by ultrasonication for one hour; to remove any unexfoliated GO, the mixture was centrifuged for ten minutes at 10 000 rpm.

After centrifugation, a brown color suspension of GO was obtained, which was then decanted and hydrothermally

reduced using hydrazine (NH_2NH_2) and ammonia solution (NH_3). In summary, ammonia was added to the solution to keep its pH in the basic range of 10, after which N_2H_4 was added and agitated for 10 minutes. Additionally, the suspension was kept in a Teflon-lined autoclave and heated to 200 °C for five hours. By repeatedly centrifuging with DW, the final black color suspension was thus achieved.

2.4 Preparation of AuNPs@rGO nanocomposite

The optimized highly stable, smaller, and isotropic AuNPs synthesized the AuNPs@rGO nanocomposite. For this purpose, 20 mL of a 0.25 mg mL^{-1} rGO solution was mixed with 2 mL of the AuNPs solution and agitated continuously for 5 hours. The resulting AuNPs@rGO nanocomposite was dried at 60 °C and centrifuged at 10 000 rpm for 15 min. To ensure purity, the nanocomposite was thoroughly washed several times with deionized water to remove residual impurities.

2.5 Peroxidase-like mimetic property of AuNPs-rGO

For examining the peroxidase-like mimetic property of the resulting NC-AuNPs, the reaction system NC-AuNPs + TMB + H_2O_2 was developed. Here, TMB was employed as a substrate for peroxidase, producing a blue color and a distinct UV-visible peak in its oxidized form at 652 nm. This experiment combined 200 μL of pH 4 NaAc buffer (0.2 M) with 50 μL TMB of 1 mM and 50 μL H_2O_2 of 1 mM. Subsequently, 50 μL of the optimally produced NC-AuNPs from AEX were combined and incubated for 60 minutes. The control experimental reactions were performed without NC-AuNPs or H_2O_2, utilising the identical reaction setup.

2.6 Detection of cholesterol

To do this, 100 μL of various concentrations of ChO in 0.1 mM PBS with pH 7.0 were first treated with 20 μL ChOx (1 mg mL^{-1}). The mixture was incubated for 10 min at 37 °C in dark conditions to form H_2O_2. Subsequently, 200 μL NaAc buffer of 0.2 M (pH 4) with 50 μL AuNPs@rGO and 50 μL TMB of 1 mM were added to the reaction mixture and incubated for another five minutes at the same temperature. Then, using a UV-visible spectrophotometer, the matching absorbance was determined at 652 nm, and digital pictures were captured.

2.7 Experimental methodology

The initial identification of the synthesis of AuNPs, GO, rGO, and AuNPs@rGO, along with the preliminary peroxidase sensing reactions, was conducted using the Evolution 201 Thermo Scientific UV-visible spectrophotometer. The important role played by the identity of functional groups was determined by using the FTIR in the range of 4000–400 cm^{-1}, specifically the PerkinElmer spectrum 100. Using an X-ray diffractometer (Rigaku Miniflex II), the crystalline properties of AuNPs and AuNPs@rGO, as well as the change in crystallinity from GO to rGO, were investigated. We examined the NC-AuNPs and the AuNPs@rGO nanocomposite's structure, size, and form using TEM (TECNAI 20 G2) at 200 kV voltage. By revealing the concentric diffraction rings, selected area electron diffraction further validated the crystallinity of AuNPs@rGO. The designed AuNPs@rGO nanocomposite exhibited mimetic activity similar to peroxidase and was utilized for colorimetric cholesterol sensing.

3. Results and discussion

3.1 Characterizations

The primary method used to confirm the synthesis of AuNPs, GO, rGO, and AuNPs@rGO was UV-visible spectroscopy, as illustrated in Fig. 1a. The typical surface plasmon resonance of AuNPs, with a λ_{max} in the 500–600 nm range, was apparent in the UV-visible spectra at 534 nm with zeta potential −11 mV (Fig. S1). Two distinctive UV-visible spectra of GO at 230 and 300 nm have appeared in Fig. 1a. The peak at 230 nm corresponded to the π–π* transition of C=C, whereas the peak present at 300 indicated the n–π* transition of C=O.[38] Fig. 1a reveals the absorption spectra of rGO, which shows a red shift from 230 nm to 270 nm, corresponding to the π–π* transition of a C=C bond. This shift indicates the successful transformation of GO into rGO due to the reduction process and restoration of a C=C bond.[39] UV-visible spectra of AuNPs@rGO nanocomposite displays peaks corresponding to both AuNPs and rGO with slight shift. The variations observed in these peaks could be attributed to the interaction between AuNPs and the surfaces of rGO, leading to the formation of the AuNPs@rGO nanocomposite. Additionally, the change in the solution's color from brown to dark black supports the chemical reduction of GO into rGO (Fig. 1a).

The synthesized AuNPs@rGO nanocomposite was further analyzed using FTIR spectroscopy to identify the functional groups associated with AuNPs, GO, rGO, and their contributions to the formation of the AuNPs@rGO nanocomposite (Fig. 1b). The FTIR spectra of AuNPs displayed distinct absorption bands at 3421, 2922, 2852, 1632, and 1061 cm^{-1}. The bands observed at 3421, 2922, and 2852 cm^{-1} correspond to the stretching vibrations (μ_s) of OH, C=C–H, and C–H functional groups, respectively, which originate from the phytochemicals present in leaf extract. Meanwhile, the 1632 and 1061 cm^{-1} peaks were attributed to the stretching vibrations of C=C and O–C bonds, respectively.[40] Similarly, the FTIR spectra of GO exhibited characteristic peaks at 3409, 2927, 2852, 1735, 1665, 1374, and 1050 cm^{-1}. These peaks were associated with the stretching vibrations of OH, sp^2 hybridized C–H, sp^3 hybridized C–H, carbonyl (C=O), C=C, C–OH, and epoxide groups, respectively.[41] The observed spectral features provided insights into the functional groups' contributions to the structural integration and stability of the AuNPs@rGO nanocomposite. The FTIR spectra of rGO revealed the shifting of 1735 cm^{-1} (C=O carbonyl) peak to 1565 cm^{-1} (sp^2 hybridized C=C) and the disappearance of 1050 cm^{-1} peak (epoxide). The disappearance of the epoxide peak (1050 cm^{-1}) and the shifting of the carbonyl peak from 1735 cm^{-1} to 1565 cm^{-1} advocated the conversion of GO to rGO by removal of surface oxygenated groups, which was aligned with the results obtained from UV-visible spectra[39,42]

Fig. 1c presents the crystalline structure analysis of the synthesized AuNPs, GO, rGO, and the AuNPs@rGO

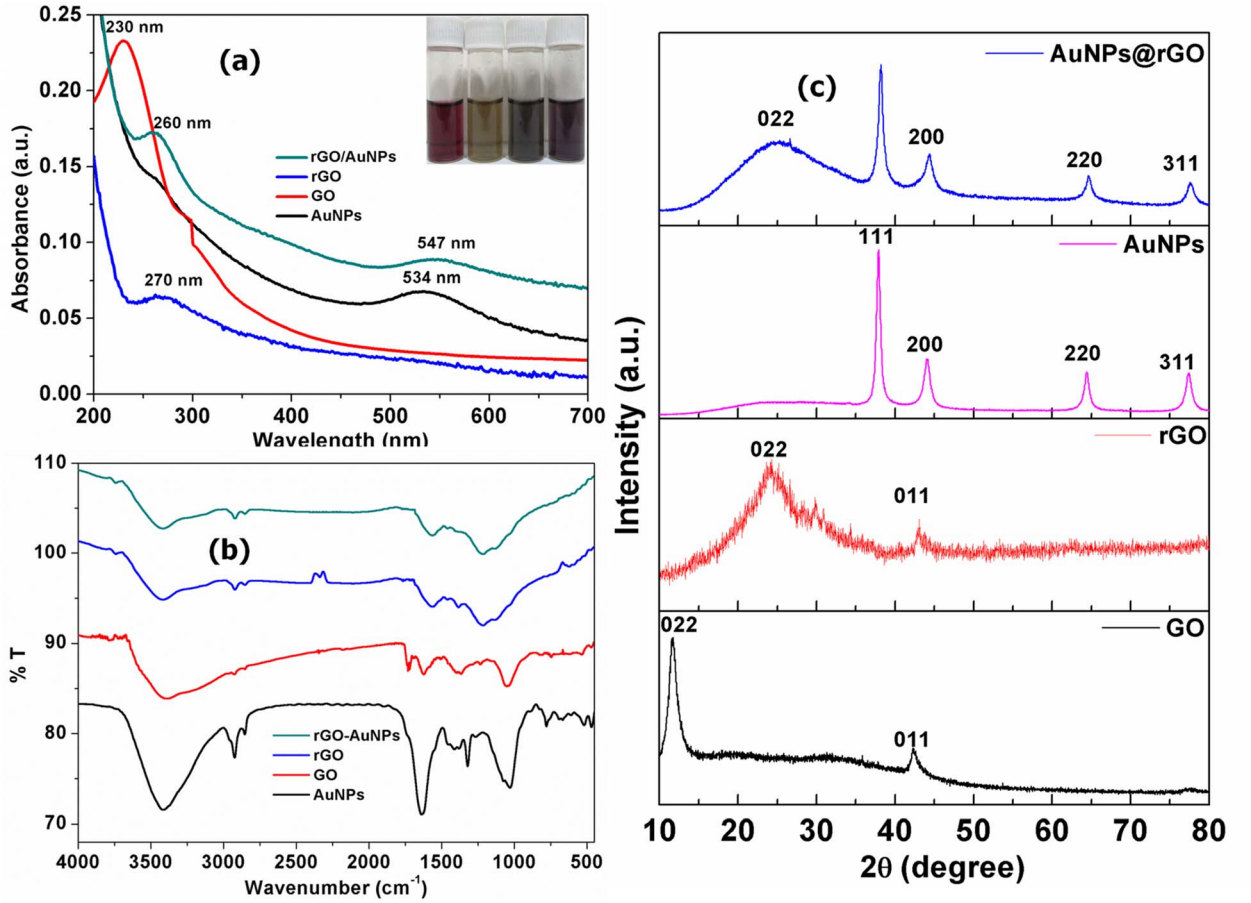

Fig. 1 (a) Characteristics UV-visible peaks of AuNPs, rGO, GO, AuNPs@rGO, (b) FTIR spectra of rGO, AuNPs, rGO, AuNPs@rGO and (c) XRD of rGO, AuNPs, GO, AuNPs@rGO.

nanocomposite, providing their phase composition. A scanning rate of 6° min^{-1} and a step size of 0.02° were used to perform XRD analysis throughout a 2θ range of 20° to 80°. Different diffraction peaks for AuNPs were seen at 2θ = 38.04°, 44.22°, 64.43°, and 77.2°, according to the findings. It was clear from these peaks that the standard JCPDS file number 040784 and corresponded to Bragg's reflections at planes (111), (200), (220), and (311), confirming the metallic gold crystalline structure with face-centered cubic (fcc) geometry. A distinctive diffraction peak of GO is visible in the XRD spectrum at 2θ = 10.9°, corresponding to 002 Bragg's reflections. The significantly increased *d*-spacing of GO (0.83 nm) compared to pure graphite (0.34 nm) indicated successful exfoliation. This exfoliation suggests the presence of water molecules and functional groups containing oxygen in the layers of graphite. On the subsequent reduction of GO, with 0.418 nm of *d*-spacing, two wide peaks at 2θ = 23.9° and 43.0°, corresponding to (002) and (011) Bragg's reflections, respectively, emerged; whereas the diffraction peak at 2θ = 10.9° vanished. The decrease in *d*-spacing of rGO was due to the elimination of intercalated oxygenated functional groups. The broadening of the peaks indicated that rGO is amorphous along the sheet's stacking direction. A distinctive peak of rGO and AuNPs in the XRD spectra of AuNPs@rGO confirmed the AuNPs-rGO nanocomposite synthesis.

Transmission electron microscopy was used to examine the AuNPs' morphology. Fig. 2a displays the transmission electron micrographs of the synthesized AuNPs, highlighting their morphology, size distribution, and structural characteristics. The images verified the existence of round gold nanoparticles with sizes ranging from 1 to 19 nm. The size distribution histogram corresponding to the TEM images revealed an average particle size of 8.6 nm, with most of the AuNPs falling within the 5–7 nm range. Fig. 2b displays the TEM image of a bare rGO sheet, which shows the absence of any AuNPs. In contrast, Fig. 2c and d, taken at different magnifications, depict the fabricated AuNPs@rGO composite. These images clearly demonstrate the uniform distribution of AuNPs on the rGO sheets and the distinct structure of the rGO, confirming the synthesis of the AuNPs@rGO composite.

3.2 Peroxidase-like activity

The peroxidase-like activity of the synthesized AuNPs, rGO, and AuNPs@rGO was investigated by monitoring a change in hue to blue resulting from the oxidation of chromogenic TMB upon its interaction with H_2O_2. Introducing AuNPs@rGO into the H_2O_2 + TMB reaction system significantly accelerates the redox process. This enhancement is attributed to the catalytic activity at the surface of AuNPs@rGO, which promotes the

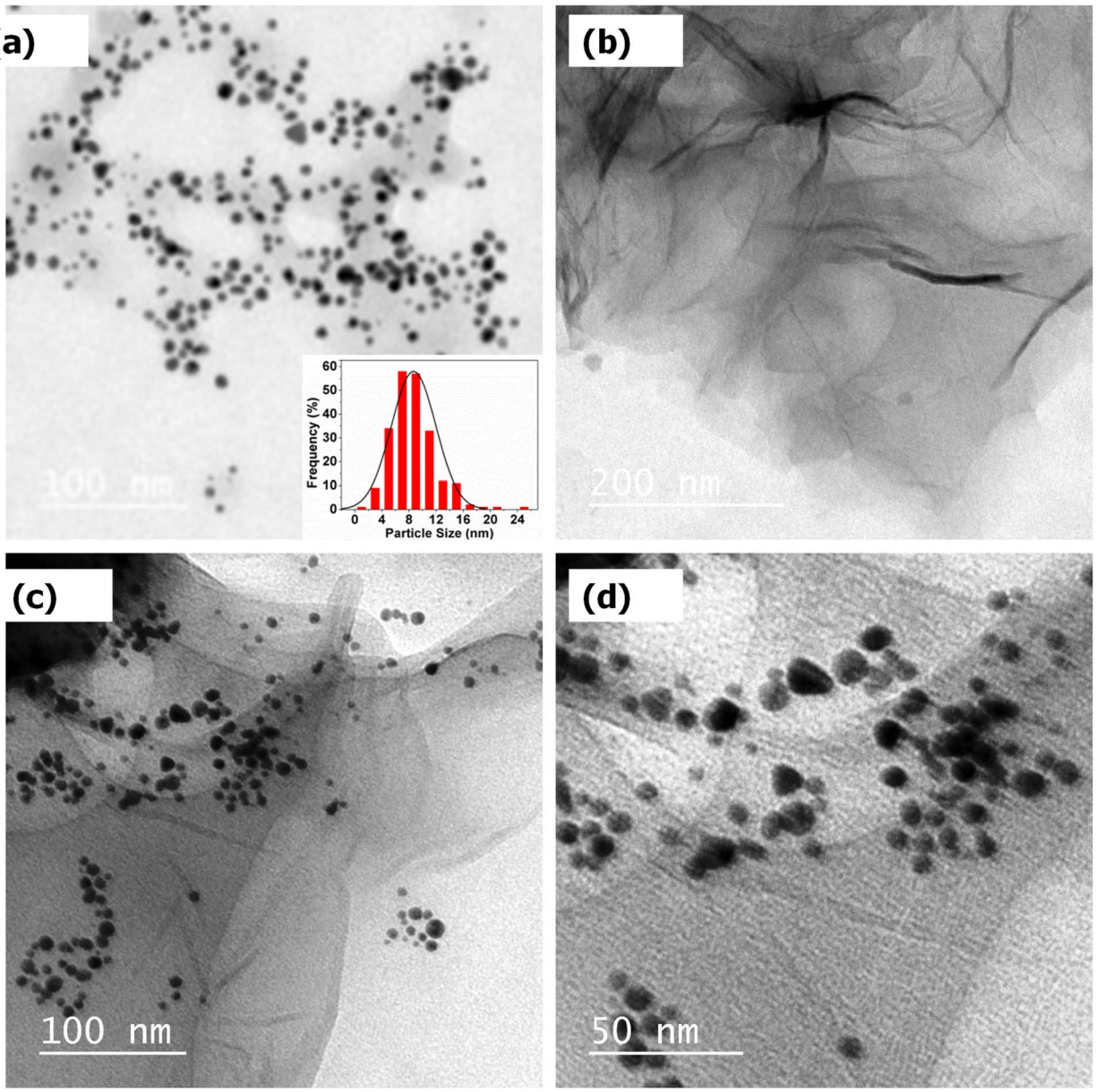

Fig. 2 HR-TEM pictures of AuNPs (a), bare rGO sheet (b–d) AuNPs@rGO at different magnifications.

decomposition of H_2O_2 into hydroxyl radicals ($OH^{\bullet}$), thereby expediting the overall reaction (Fig. 3a).[21]

The generated $OH^{\bullet}$ radical extracts the electron from the reduced TMB and turns it into the dark blue oxTMB with a characteristic absorbance of 652 nm. The catalytic action of the ChOx on ChO releases H_2O_2 and cholest-4ene-3-one as a by-product with the help of oxygen.[43] The produced H_2O_2 in this reaction can be used quantitatively to oxidize TMB into oxTMB in the presence of AuNPs@rGO (Fig. 3a). This fact encouraged us to use colorimetric methods for the detection of cholesterol.

The peroxidase-like activity of AuNPs, rGO, and AuNPs@rGO was investigated by regularly observing the UV-visible peaks of the oxidized blue color product of TMB, which gives sharp spectra at 652 nm. The figure shows that the absence of the characteristic peak of the OxTMB at 652 nm indicated that the rGO could not independently mimic peroxidase activity (Fig. 3b). This was caused by the fused layers of rGO, which hinder the adsorption of substrates onto its surface and prevent the transfer of electrons.[44] Although the AuNPs exhibited spectra at 652 nm, they were not as intense as those of AuNPs@rGO, indicating the superior catalytic activity of AuNPs@rGO.

To investigate the role of each constituent in various compositions (H_2O_2, TMB, TMB + H_2O_2, AuNPs@rGO + TMB, and AuNPs@rGO + TMB + H_2O_2) in developing a dark blue color and the intense absorption of OxTMB at a wavelength of 652 nm, the time-dependent changes in absorbance were systematically monitored (Fig. 3c). The absorbance spectra of H_2O_2, TMB alone, and AuNPs@rGO + TMB without H_2O_2 showed no significant changes over time. In contrast, the

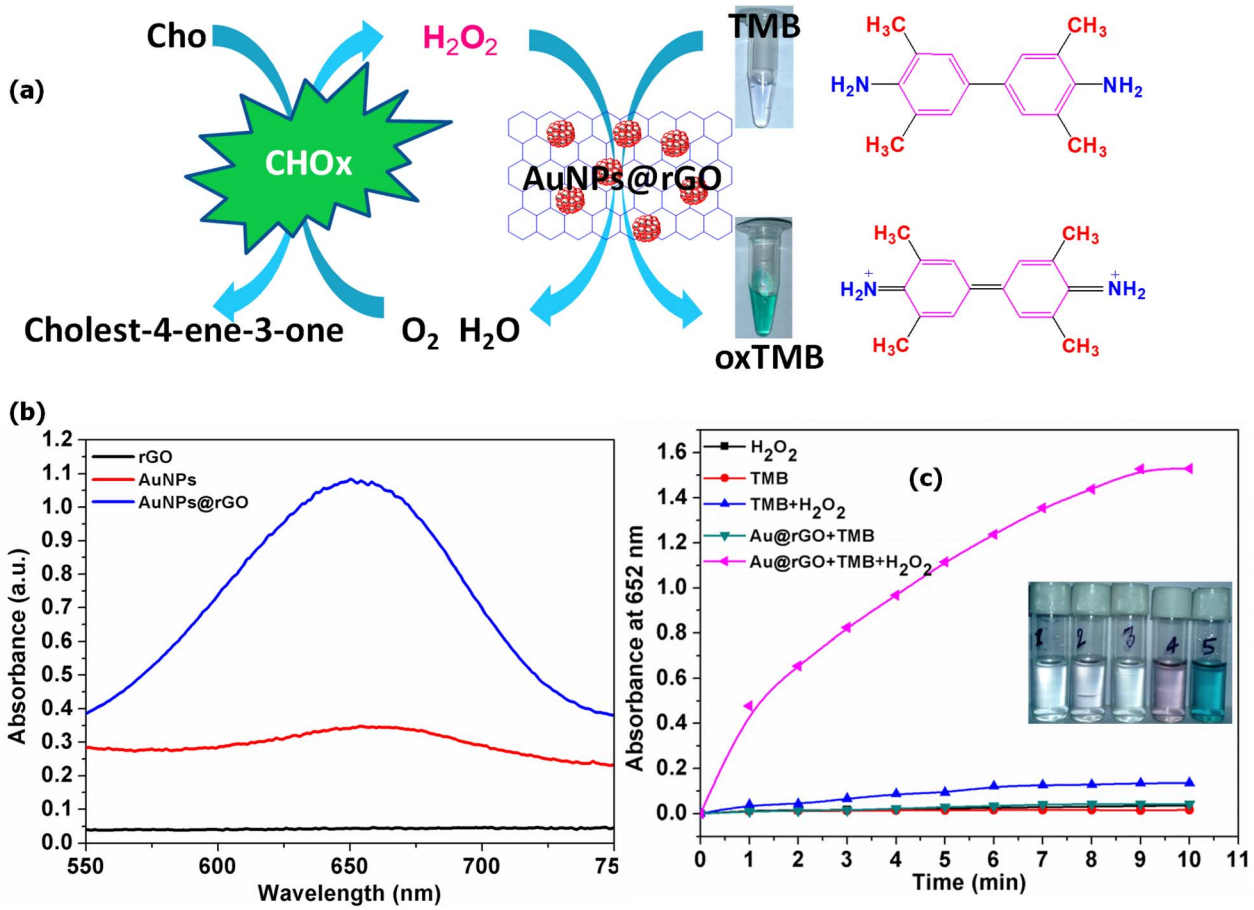

Fig. 3 (a) Schematic of AuNPs@rGO peroxidase-like activity for colorimetric cholesterol sensing; (b) UV-vis spectra of rGO, AuNPs, and AuNPs@rGO with TMB and H_2O_2; (c) absorbance at 652 nm for different reaction mixtures, with inset showing color changes.

absorbance spectra for the TMB + H_2O_2 system exhibited only minor alterations at 652 nm, attributable to the low reactivity between TMB and H_2O_2. However, a pronounced change was observed when AuNPs@rGO was inserted into the TMB + H_2O_2. The reaction yielded a deep blue color (Inset, Fig. 3c) and a substantial increase in absorbance at 652 nm within 1 minute, which continued to intensify for up to 9 minutes. This result provides strong evidence of the peroxidase-like activity of AuNPs@rGO.

3.3 Optimization of process parameters

It is commonly known that temperature and pH levels significantly impact the catalytic activity of natural enzymes. Furthermore, variations in the concentration of the components of the reaction system also impact the catalytic activity of natural enzymes. By holding one parameter constant at a time, the many factors that affect the peroxidase-like catalytic activity of AuNPs@rGO inclusive of incubation duration, temperature, TMB concentration, pH, H_2O_2 concentration, and AuNPs amount were optimized to achieve the best result for the improved performance of cholesterol detection. Fig. 4 a show the effect of pH on the catalytic potential of AuNPs@rGO in 0.2 M NaAc buffer at different pH ranges of 1–10. The figure corroborated that the artificial enzyme-like potential of AuNPs@rGO was excellent under an acidic medium and the optimum pH of 4.

The ability of AuNPs@rGO to mimic peroxidase began to decline with a further increase in pH, becoming negligible at higher pH levels. This behavior can be attributed to the decomposition of H_2O_2 at elevated pH, leading to the generation of H_2O and O_2 molecules instead of $OH^{\bullet}$ radicals. Similarly, adjusting the temperature of AuNPs@rGO to enhance its peroxidase-like activity was evaluated, revealing that the activity was optimal at 40 °C. Beyond this temperature, the activity diminished, primarily due to the agglomeration of AuNPs@rGO, which inhibited electron transfer[45] (Fig. 4b). Additionally, the impact of various constituents in the AuNPs@rGO reaction system, such as the amount of AuNPs@rGO and the concentrations of TMB and H_2O_2, was systematically optimized. These optimizations were performed under constant conditions, including an incubation time of 9 minutes, pH 4, and a temperature of 40 °C. Excessively high or low concentrations of TMB, H_2O_2, or the amount of AuNPs@rGO were unsuitable for enhancing peroxidase activity of AuNPs@rGO. During optimization, 0.8 mM TMB was identified as the optimal concentration when combined with 50 μL of H_2O_2 in 200 μL of NaAc buffer with 50 μL of AuNPs@rGO and

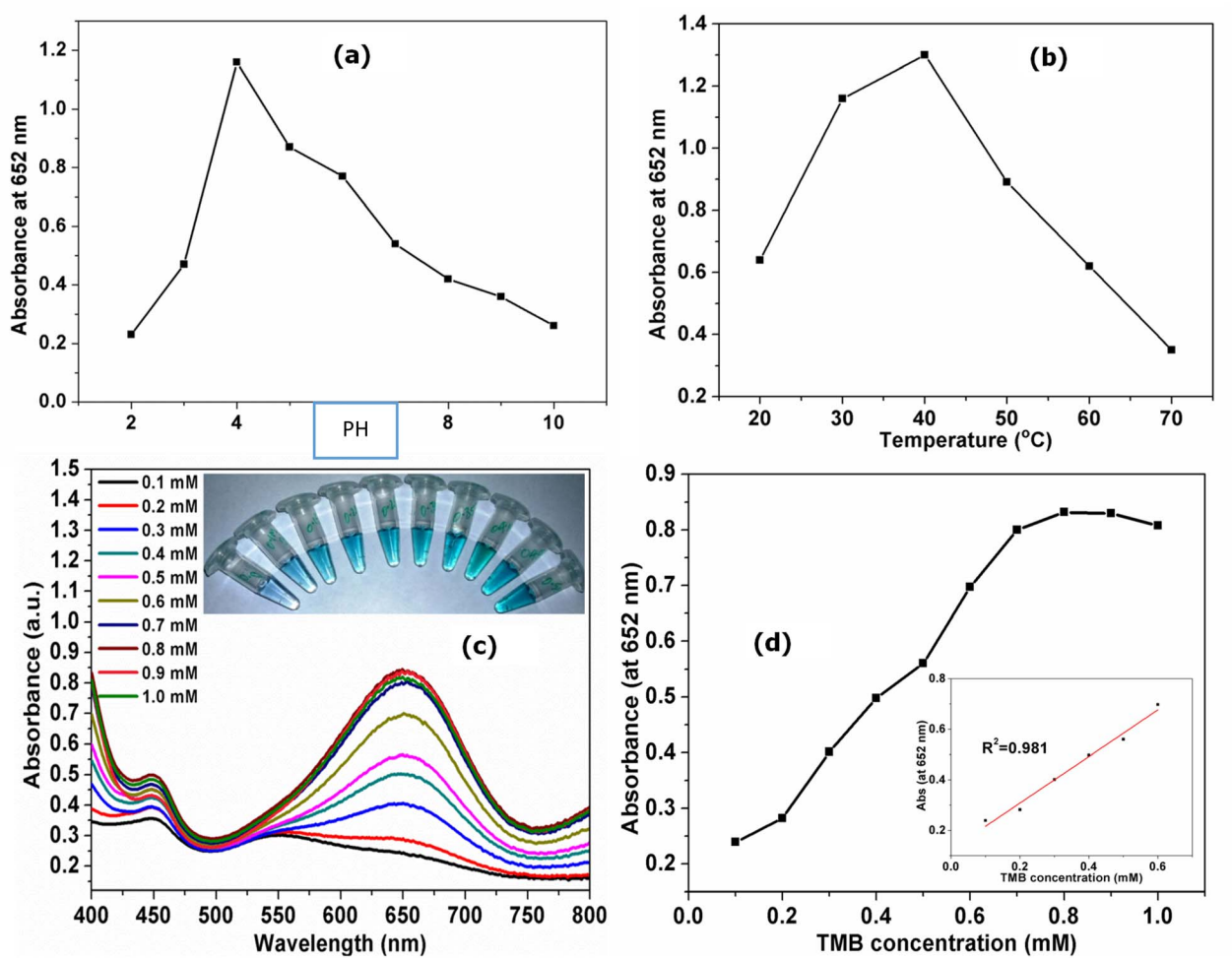

Fig. 4 Peroxidase-like activity of AuNPs@rGO under varying (a) pH (2–10) at 36 °C, (b) temperatures (20–70 °C), (c) TMB concentrations (0.1–1 mM) at pH 4 and 40 °C with color change inset, and (d) absorbance *vs.* TMB concentration with linear calibration inset (R^2 = 0.993).

1 mM of NaCl. This combination produced the best peroxidase activity of AuNPs@rGO (Fig. 4c). Additionally, the inset in Fig. 4d demonstrates a linear relationship between TMB concentrations of 0.1 and 0.6 mM, with a correlation coefficient (R^2) of 0.981.

Fig. 5a and b demonstrate that 80 μL of AuNPs@rGO was optimal for achieving improved peroxidase-like activity when employing 50 μL H_2O_2 (1 mM) and 50 μL TMB (0.8 mM) were used, and a linear connection was found between 10 and 60 μL AuNPs@rGO, with an R^2 value of 0.997. An 8 mM concentration of H_2O_2 was identified as the optimal level when using 80 μL of gold nanoparticles immobilized on red GO, along with 50 μL of TMB (0.8 mM), as demonstrated in Fig. 5c and d. Fig. 5d exhibits the linear calibration plot of H_2O_2, which shows between 0.1 mM and 0.6 mM, there is a linear correlation, with an *R*-value of 0.997. The linear regression equation is $A_{652\ nm}$ = 1.510C + 0.618, and the limit of detection (LOD) of H_2O_2 is found to be 0.0268 mM. This H_2O_2 can be generated through the catalytic oxidation of cholesterol using a catalyst like cholesterol oxidase (ChOx), which encouraged us to develop the facile colorimetric detection method of cholesterol (Fig. 5d).

3.4 Detection of cholesterol

After the detection of H_2O_2, the efficacy of the fabricated AuNPs@rGO was applied to detect the cholesterol selectively and sensitively by quantifying the released H_2O_2 through the catalytic action of ChOx on ChO. For the detection purpose, different concentrations after adding 20 μL of ChOx (1 mg mL^{-1}) to 100 μL of Tris–HCl buffer (20 mM, pH 7.0), the remaining ChO was handled similarly followed by the addition of the optimum component of the reaction system, *i.e.*, 50 μL AuNPs@rGO and 50 μL 200 μL of 0.1 mM NaAc buffer solutions with 0.8 mM TMB and a pH of 4.0. The UV-visible spectra were subsequently recorded at 652 nm, where maximum absorbance was observed. Using the absorbance data at this wavelength, a calibration curve for ChO was constructed, demonstrating connecting 0.2 and 1.2 mM on a straight line with a R^2 of value of 0.996. The linear regression equation for the curve is $A_{652\ nm}$ = 0.547C + 0.170A. The limit of detection (LOD) was determined to be 0.062 mM using the equation LOD = 3(SD/B), where SD represents the standard deviation and B denotes the slope of the calibration curve (Fig. 6a and b). This LOD is satisfactory compared to previously reported values, as summarized in Table 1.

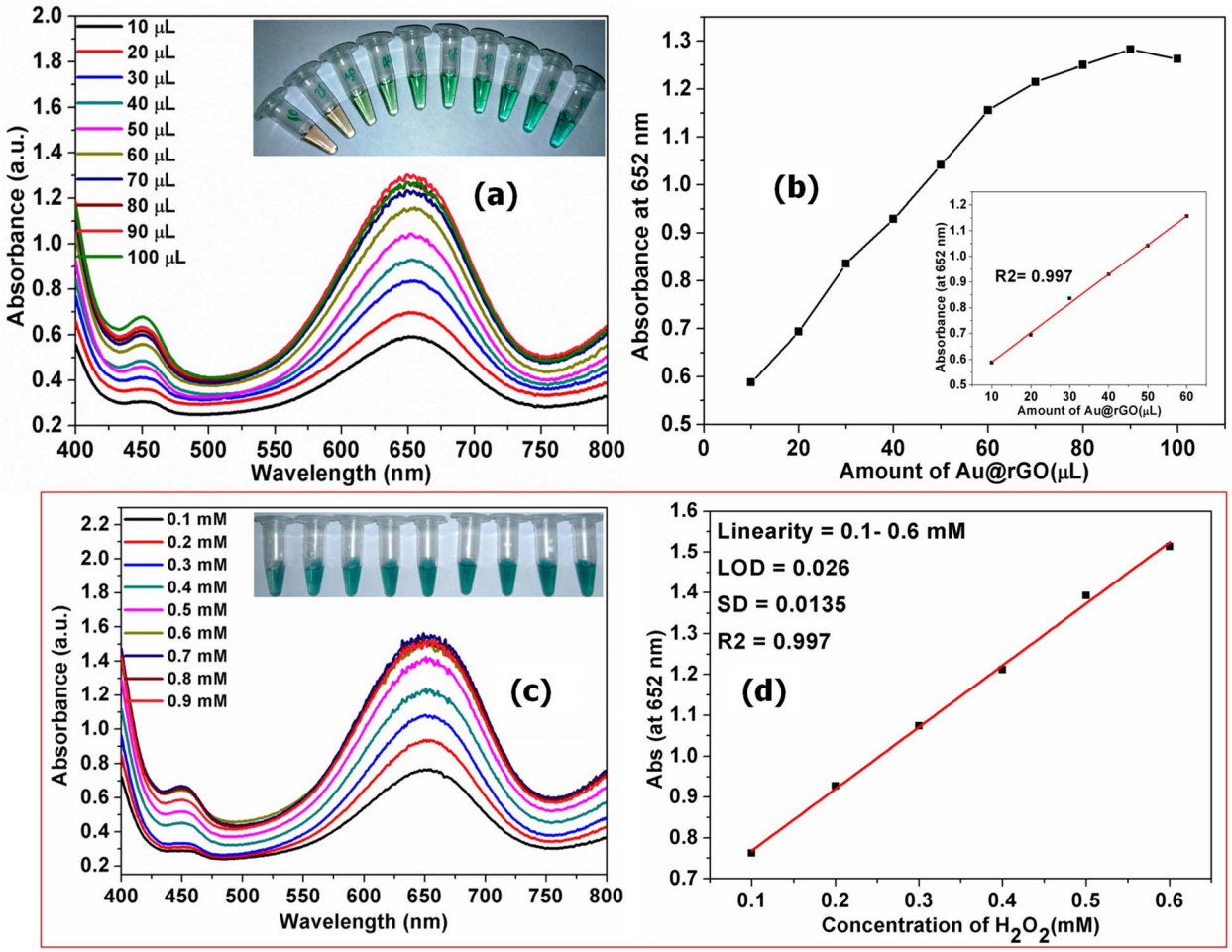

Fig. 5 Peroxidase-mimicking activity of AuNPs@rGO: (a) effect of nanocomposite volume with color change inset, (b) linear response from 10–60 µL ($R^2 = 0.997$), (c) effect of H_2O_2 concentration with color change inset, (d) linear response from 0.1–0.6 mM ($R^2 = 0.997$).

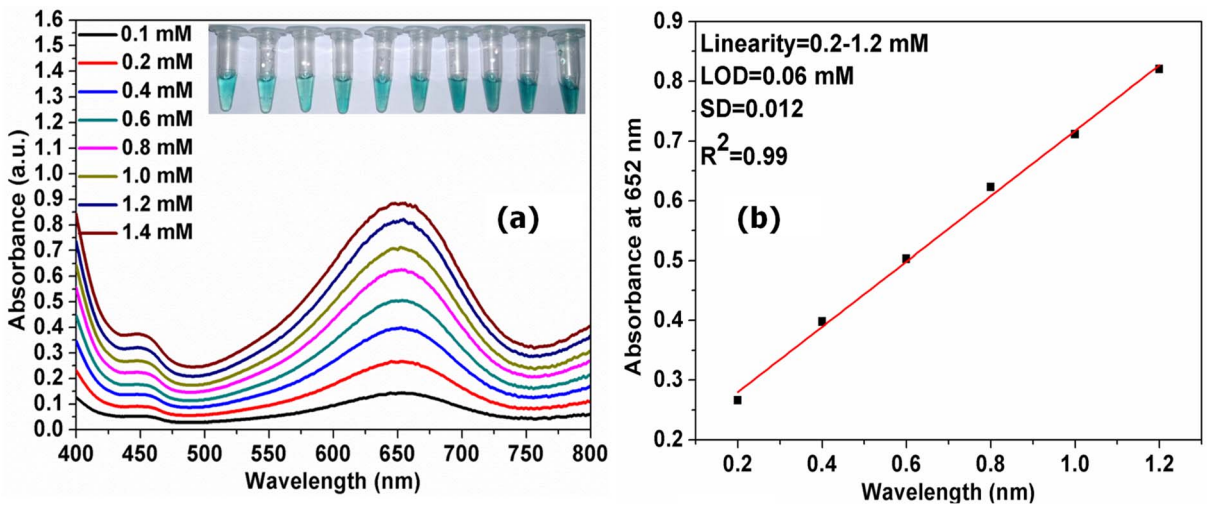

Fig. 6 (a) UV-vis spectra of different ChO concentrations in the AuNPs@rGO + TMB + ChOx system; (b) calibration curve showing a linear range from 0.2–1.2 mM ($R^2 = 0$).

Table 1 Comparison table showing the different materials used for the detection of ChO

Sensing system	Sensing technique	Linear range	LOD	Reference
ChOx/DNAzymes	Colorimetric	1–30 mM	0.1 M	45
MMSNs/ChOx	Colorimetric	0.01–0.3 M	7.12 μM	46
MoS_2 NR-Au NP	Colorimetric	0.04–1.0 mM	0.015 mM	47
Pt/PCN	Colorimetric	—	8.3×10^{-6} M	9
ChOx/haemoglobin	Amperometric	10–600 M	9.5 M	27
AuNPs@rGO	Colorimetric	0.2 to 1.2 mM	0.062 mM	Present work

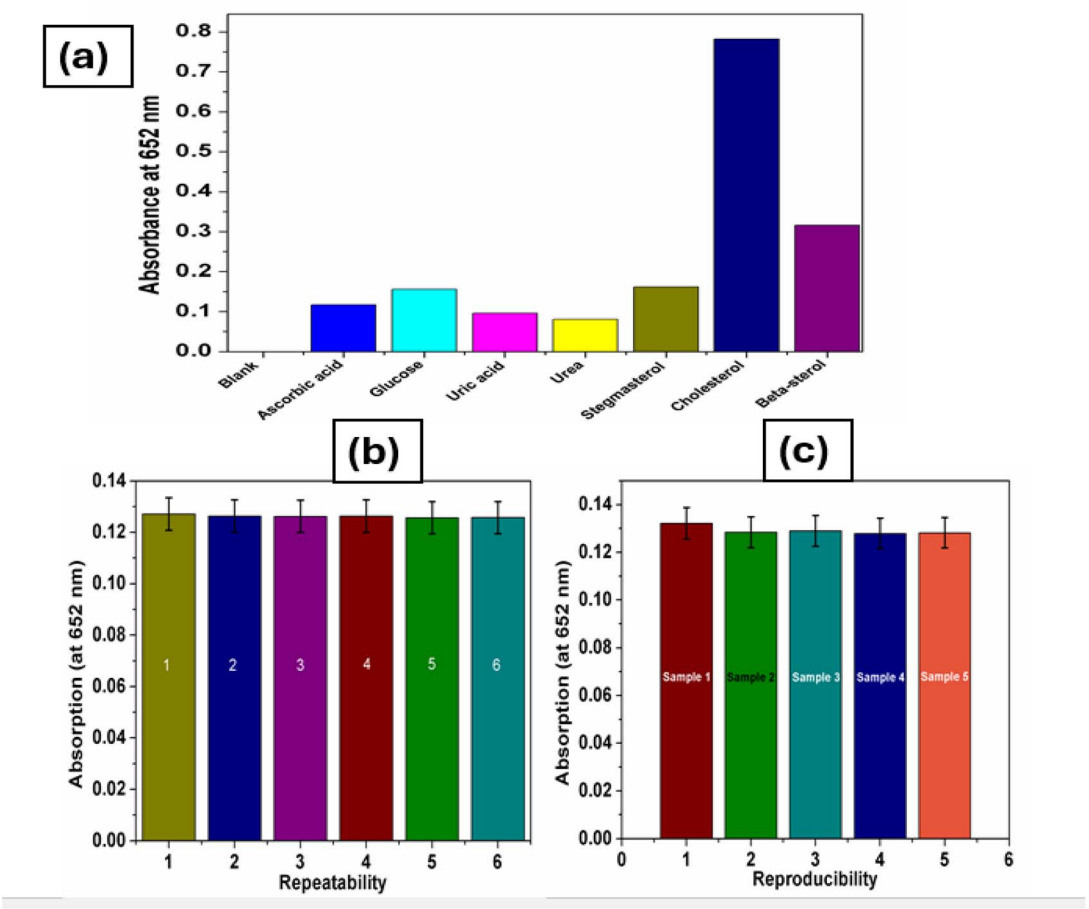

Fig. 7 (a) Selectivity of AuNPs@rGO toward ChO over other analytes; (b and c) repeatability and reproducibility of the assay under identical condition.

3.5 Selectivity

To evaluate the selectivity of the fabricated AuNPs@RGO, an experiment was conducted by adding 50 μL of 1 mM solutions of various potential analytes found in blood serum such as ascorbic acid, uric acid, xanthine, urea, beta-sitosterol, stigmasterol, and cholesterol into the same reaction system used for ChO detection (Fig. 7a). The results show that ChO demonstrated the highest selectivity, with its absorbance intensity being the strongest among all the tested analytes. The fabricated system demonstrates the potential for selective colorimetric sensing of ChO. Fig. 7b illustrates the consistency of results obtained from the fabricated AuNPs@rGO system when the experiment was repeated six times under identical experimental conditions. Similarly, Fig. 7c shows the reproducibility of results across five samples tested under the same experimental setup.

4. Conclusion

This study highlights the successful development of AuNPs@rGO with exceptional peroxidase-like mimicking activity using a green synthesis approach. Negatively charged AuNPs and rGO, synthesized *via* the reduction of GO, were combined to create the AuNPs@rGO composite. Characterization techniques, including TEM, FTIR, XRD, and UV-visible spectroscopy, confirmed the efficient synthesis and uniform distribution of AuNPs on the rGO sheets. The catalytic activity of

AuNPs@rGO was optimized by analyzing the effects of pH, temperature, TMB concentration, and material quantity, demonstrating significant efficiency under acidic conditions and at 40 °C. The synthesized material was effectively utilized for the colorimetric detection of H_2O_2 and cholesterol with detection limits of 0.0268 mM and 0.062 mM, respectively. This cost-effective, rapid, highly selective, and sensitive method offers a capable approach for cholesterol detection, with potential applications in medical diagnostics and treatment.

Conflicts of interest

The authors declare no competing financial or personal interests influencing this work.

Data availability

All data analyzed during the study are included in this article and will be made available upon reasonable request.

Supplementary information (SI) is available. See DOI: https://doi.org/10.1039/d5ra07564e.

Funding

This research was funded by Taif University, Saudi Arabia, Project No. (TU-DSPP-2025-44).

Acknowledgements

The authors extend their appreciation to Taif University, Saudi Arabia, for supporting this work through project number (TU-DSPP-2025-44).

References

1 O. Domínguez-Renedo, A. M. Navarro-Cunado and M. A. Alonso-Lomillo, Electrochemical devices for cholesterol detection, *J. Pharm. Biomed. Anal.*, 2023, **224**, 115195.
2 M. A. H. Nawaz, *et al.*, Development of a disposable electrochemical sensor for detection of cholesterol using differential pulse voltammetry, *J. Pharmaceut. Biomed. Anal.*, 2018, **159**, 398–405.
3 J. Kim, *et al.*, Development of an electrochemical biosensor for non-invasive cholesterol monitoring via microneedle-based interstitial fluid extraction, *Talanta*, 2024, **280**, 126771.
4 L. Gao, *et al.*, Intrinsic peroxidase-like activity of ferromagnetic nanoparticles, *Nat. Nanotechnol.*, 2007, **2**(9), 577–583.
5 M. Sadiq, *et al.*, MXene-montmorillonite nanocomposites-based scaffold sensors for early pancreatic cancer diagnosis, *Cancer Plus*, 2024, **6**(3), 3793.
6 J. Yin, H. Cao and Y. Lu, Self-assembly into magnetic Co 3 O 4 complex nanostructures as peroxidase, *J. Mater. Chem.*, 2012, **22**(2), 527–534.
7 B. Shobana and P. Prakash, Ultrasensitive and Selective Nanomolar Detection of Aceclofenac Using Bi2O3/CeO2@B-NQds-Modified Electrodes Through an Advanced Photoelectrocatalytic Approach, *Electrocatalysis*, 2025, **16**(3), 462–477.
8 Y. Wang, *et al.*, Bifunctionalized novel Co-V MMO nanowires: Intrinsic oxidase and peroxidase like catalytic activities for antibacterial application, *Appl. Catal., B*, 2020, **261**, 118256.
9 W. Shi, *et al.*, Pd nanoparticles supported on nitrogen, sulfur-doped three-dimensional hierarchical nanostructures as peroxidase-like catalysts for colorimetric detection of xanthine, *RSC Adv.*, 2015, **5**(41), 32183–32190.
10 Y. Jv, B. Li and R. Cao, Positively-charged gold nanoparticles as peroxidiase mimic and their application in hydrogen peroxide and glucose detection, *Chem. Commun.*, 2010, **46**(42), 8017–8019.
11 J. Yan, *et al.*, Aptamer based photometric assay for the antibiotic sulfadimethoxine based on the inhibition and reactivation of the peroxidase-like activity of gold nanoparticles, *Microchim. Acta*, 2017, **184**(1), 59–63.
12 V. Kumar, M. Shariq, D. Alhashmialameer, *et al.*, Green synthesis of gold nanoparticles using Xanthium strumarium extract: photoinduced fabrication, characterization, and biosensing applications, *Res. Chem. Intermed.*, 2025, **51**, 5079–5100.
13 W. Zhang, *et al.*, In vitro cytotoxicity evaluation of graphene oxide from the peroxidase-like activity perspective, *Colloids Surf., B*, 2017, **151**, 215–223.
14 W. Yang, *et al.*, Photo-switchable peroxidase/catalase-like activity of carbon quantum dots, *Angew. Chem.*, 2024, **136**(22), e202403581.
15 V. Kumar, *et al.*, Size-dependent synthesis of gold nanoparticles and their peroxidase-like activity for the colorimetric detection of glutathione from human blood serum, *ACS Sustain. Chem. Eng.*, 2018, **6**(6), 7662–7675.
16 M. Hussain, *et al.*, Efficient adsorptive removal of methyl red dye using a novel myrrh/GO-TiO Nano-adsorbent: Synthesis, characterization, and adsorption studies, *Diamond Relat. Mater.*, 2026, **161**, 113131.
17 X. Chen, *et al.*, Au nanoparticles on citrate-functionalized graphene nanosheets with a high peroxidase-like performance, *Dalton Trans.*, 2014, **43**(20), 7449–7454.
18 X. Li, *et al.*, Enzyme mimics based on self-assembled peptide functionalized with graphene oxide for polyethylene terephthalate degradation, *Colloids Surf., B*, 2025, **251**, 114588.
19 Y. Zheng, *et al.*, Sulfur-doped g-C3N4/rGO porous nanosheets for highly efficient photocatalytic degradation of refractory contaminants, *J. Mater. Sci. Technol.*, 2020, **41**, 117–126.
20 H. Zhang, D. Hines and D. L. Akins, Synthesis of a nanocomposite composed of reduced graphene oxide and gold nanoparticles, *Dalton Trans.*, 2014, **43**(6), 2670–2675.
21 L. A. Al-Ani, *et al.*, Graphene–gold based nanocomposites applications in cancer diseases; Efficient detection and therapeutic tools, *Eur. J. Med. Chem.*, 2017, **139**, 349–366.
22 O. Sadak, One-pot scalable synthesis of rGO/AuNPs nanocomposite and its application in enzymatic glucose biosensor, *Nanocomposites*, 2021, **7**(1), 44–52.

23 M. Liu, *et al.*, Stimuli-responsive peroxidase mimicking at a smart graphene interface, *Chem. Commun.*, 2012, **48**(56), 7055–7057.
24 J. Dolai, A. Modak and N. R. Jana, Nanocomposite with imprint of cholesterol for its nonenzymatic, visual, and smartphone-based detection, *ACS Appl. Eng. Mater.*, 2022, **1**(1), 428–435.
25 N. R. Nirala, *et al.*, Colorimetric detection of cholesterol based on highly efficient peroxidase mimetic activity of graphene quantum dots, *Sens. Actuators, B*, 2015, **218**, 42–50.
26 S. Wu, *et al.*, Gold nanoparticles/single-stranded DNA-reduced graphene oxide nanocomposites based electrochemical biosensor for highly sensitive detection of cholesterol, *Front. Chem. Sci. Eng.*, 2021, **15**(6), 1572–1582.
27 O. Demkiv, *et al.*, The peroxidase-like nanocomposites as hydrogen peroxide-sensitive elements in cholesterol oxidase-based biosensors for cholesterol assay, *J. Funct. Biomater.*, 2023, **14**(6), 315.
28 Y. Wu, *et al.*, Metal-organic framework coated Fe3O4 magnetic nanoparticles with peroxidase-like activity for colorimetric sensing of cholesterol, *Sens. Actuators, B*, 2017, **249**, 195–202.
29 Q. Sun, *et al.*, Fluorometric detection of cholesterol based on β-cyclodextrin functionalized carbon quantum dots via competitive host-guest recognition, *Talanta*, 2017, **167**, 513–519.
30 C. H. Grün and S. Besseau, Normal-phase liquid chromatography–atmospheric-pressure photoionization–mass spectrometry analysis of cholesterol and phytosterol oxidation products, *J. Chromatogr. A*, 2016, **1439**, 74–81.
31 H. Liu, *et al.*, Optical determination of cholesterol in milk with molecularly imprinted polymer-coated quantum dots, *Anal. Lett.*, 2017, **50**(12), 1964–1976.
32 N. Ayyandurai, S. Venkatesan and S. Raman, A sensitive enzymatic electrochemical biosensor for cholesterol based on cobalt ferrite@ molybdenum disulfide/gold nanoparticles, *ACS Appl. Bio Mater.*, 2024, **7**(6), 4080–4092.
33 Y. He, *et al.*, Photometric determination of free cholesterol via cholesterol oxidase and carbon nanotube supported Prussian blue as a peroxidase mimic, *Microchim. Acta*, 2017, **184**(7), 2181–2189.
34 C. Wu, *et al.*, Rapid, direct analysis of cholesterol by charge labeling in reactive desorption electrospray ionization, *Anal. Chem.*, 2009, **81**(18), 7618–7624.
35 Y. Zhang, *et al.*, Boron nitride nanosheet/CuS nanocomposites as mimetic peroxidase for sensitive colorimetric detection of cholesterol, *Sens. Actuators, B*, 2017, **246**, 118–126.
36 D. K. Singh, *et al.*, Modeling of adsorption behavior of the amine-rich GOPEI aerogel for the removal of As (III) and As (V) from aqueous media, *RSC Adv.*, 2016, **6**(61), 56684–56697.
37 M. Javed, *et al.*, Synergistic influences of doping techniques and well-defined heterointerface formation to improve the photocatalytic ability of the S-ZnO/GO nanocomposite, *ChemistrySelect*, 2022, **7**(29), e202201913.
38 D. Bano, *et al.*, Green synthesis of fluorescent carbon quantum dots for the detection of mercury (II) and glutathione, *New J. Chem.*, 2018, **42**(8), 5814–5821.
39 S. Mohan, *et al.*, Effective removal of lead ions using graphene oxide-MgO nanohybrid from aqueous solution: isotherm, kinetic and thermodynamic modeling of adsorption, *J. Environ. Chem. Eng.*, 2017, **5**(3), 2259–2273.
40 H. Gao, *et al.*, One-step electrochemical synthesis of PtNi nanoparticle-graphene nanocomposites for nonenzymatic amperometric glucose detection, *ACS Appl. Mater. Interfaces*, 2011, **3**(8), 3049–3057.
41 W. Shi, *et al.*, Honeycomb-like nitrogen-doped porous carbon supporting Pt nanoparticles as enzyme mimic for colorimetric detection of cholesterol, *Sens. Actuators, B*, 2015, **221**, 1515–1522.
42 S. Babu, R. Kathirvel and P. Periakaruppan, A glassy carbon electrode modified with gold decorated iron oxide/carbon dots for light assisted voltammetric detection of antibiotic resistant microbe Enterococcus faecalis, *Biosens. Bioelectron.:X*, 2024, **20**, 100532.
43 C. Cai, *et al.*, Molecular Network-Bearing Fe–N–C Single-Atom Nanozymes for Monitoring Intracellular Glutathione Fluctuations, *ACS Appl. Nano Mater.*, 2024, **7**(8), 9507–9517.
44 S. Mohan, *et al.*, Synthesis and characterization of rGO/ZrO 2 nanocomposite for enhanced removal of fluoride from water: kinetics, isotherm, and thermodynamic modeling and its adsorption mechanism, *RSC Adv.*, 2016, **6**(90), 87523–87538.
45 R. Li, *et al.*, Colorimetric detection of cholesterol with G-quadruplex-based DNAzymes and ABTS2−, *Anal. Chim. Acta*, 2012, **724**, 80–85.
46 X. Wang, *et al.*, Mesoporous silica-stabilized magnetite nanoparticles with peroxidase-like activities for sensitively detecting cholesterol in animal-derived foods, *Colloids Surf., B*, 2024, **233**, 113653.
47 N. R. Nirala, *et al.*, Different shades of cholesterol: Gold nanoparticles supported on MoS2 nanoribbons for enhanced colorimetric sensing of free cholesterol, *Biosens. Bioelectron.*, 2015, **74**, 207–213.